Formation of Well-Ordered Heterojunctions in Polymer:PCBM Photovoltaic Devices

Ximin He, Feng Gao, Guoli Tu, David G. Hasko, Sven Hüttner, Neil C. Greenham, Ullrich Steiner,* Richard H. Friend,* and Wilhelm T. S. Huck**

The nanoscale morphology in polymer:PCBM based photovoltaic devices is a major contributor to overall device performance. The disordered nature of the phase-separated structure, in combination with the small length scales involved and the inherent difficulty of reproducing the exact morphologies when spin-coating and annealing thin blend films, have greatly hampered the development of a detailed understanding of how morphology impacts photovoltaic device functioning. In this paper we demonstrate a double nanoimprinting process that allows the formation of nanostructured polymer:PCBM heterojunctions of composition and morphology that can be selected independently. We fabricated photovoltaic (PV) devices with extremely high densities (10^{14} mm^{-2}) of interpenetrating nanoscale columnar features (as small as 25 nm; at or below the exciton diffusion length) in the active layer. By comparing device results of different feature sizes and two different polymer:PCBM combinations, we demonstrate how double imprinting can be a powerful tool to systematically study different parameters in polymer photovoltaic devices.

1. Introduction

Organic photovoltaic cells are a promising route to low-cost conversion of solar energy into electrical energy.[1] To date the most efficient devices are achieved using blends of a conjugated polymer and methanofullerene, with efficiencies of order 6–7% under solar conditions.[2,3] However, the search for new materials is greatly hampered by the difficulty of controlling the nanoscale morphology and the resulting difficulty in predicting the exact contributions from the photophysical processes occurring in devices. In solar cells based on semiconducting polymers, photons incident on the active layer create excitons (electron-hole pairs) that first need to dissociate into free charge carriers at the donor/acceptor (D/A) interface. In most pristine semiconducting polymers cast from solution, these excitons can diffuse less than 10–20 nm before decaying to the ground state.[4–6] The formation of nanoscale phase separated interpenetrating networks of donor and acceptor polymers is of paramount importance in polymer bulk heterojunction (BHJ) solar cells.[7] Furthermore, if the free charges are confined to domains that are isolated from the appropriate electrode or if the carriers are too far from the electrode, they will eventually recombine at a BHJ interface. Thus, for the mobile carriers to contribute to the photocurrent, the domain in which they form must be in contact with the appropriate electrode. Because of this necessity for fully bicontinuous interpenetrating networks comprising the donor and acceptor materials and the weak intermolecular forces between the molecular partners, these devices are acutely sensitive to processing conditions. A significant amount of work has been devoted to optimizing phase separation and crystallization of polymer/fullerene blends by altering film casting conditions. The film morphology can then be further optimized through thermal annealing, which leads to better order within the P3HT and demixing of the blend.[8,9] Other techniques, such as slow drying,[8] solvent annealing,[10] the use of processing additives,[11] and aggregation in solution[12] have also led to increased performance by allowing a degree of control over the polymer packing and polymer/fullerene phase separation during the film formation process.

While ideal photovoltaic structures have been proposed with interdigitated, pure phases spaced by a distance equal to or less than the exciton diffusion length, there are few experimental reports where this type of nanostructure is directly controlled and the effect on photovoltaic performance is investigated.[13]

X. He, Prof. W. T. S. Huck
The Nanoscience Centre
University of Cambridge
11 J. J. Thomson Avenue, Cambridge CB3 0FF, United Kingdom.
E-mail: wtsh2@cam.ac.uk
X. He, Dr. G. Tu, Prof. W. T. S. Huck
Melville Laboratory
Department of Chemistry
University of Cambridge
Lensfield Road, Cambridge CB2 1EW, United Kingdom
Dr. F. Gao, Dr. D. G. Hasko, Dr. S. Hüttner, Prof. N. C. Greenham, Prof. U. Steiner, Prof. R. H. Friend
Cavendish Laboratory
Department of Physics
University of Cambridge
J. J. Thomson Avenue, Cambridge CB3 0FF, United Kingdom
E-mail: ncg11@cam.ac.uk; u.steiner@phy.cam.ac.uk; rhf10@cam.ac.uk
Prof. W. T. S. Huck
Radboud University Nijmegen
Institute for Molecules and Materials
Heyendaalseweg 135, 6525 AJ Nijmegen, The Netherlands

DOI: 10.1002/adfm.201000573

Recently, we demonstrated the use of a new double imprinting strategy to create interdigitated D/A structures with features in the 25 nm to 200 nm size range and investigated the influence of feature size on device performance for all-polymer (P3HT and poly((9,9-dioctylfluorene)-2,7-diyl-alt-[4,7-bis(3-hexylthien-5-yl)-2,1,3-benzothiadiazole]-2′,2″-diyl) (F8TBT)) photovoltaic (PV) devices.[14] Here, we will further extend our technique to include polymer-fullerene based devices.

Nanoimprint lithography has been explored by several groups as a route to produce nanoscale features in both polymer-based and hybrid organic-inorganic PV cells.[15–18] In the case of the polymer-based devices, small improvements in device performance were observed when nanoscale gratings were imprinted into the polymer film, followed by crosslinking of the features and evaporating or spin-coating acceptor material. The drawbacks of these methods were the rather large imprinted feature sizes (by far exceeding the exciton diffusion lengths), the detrimental crosslinking treatment, and the high-temperature deposition process which completes the photovoltaic cell. The advantage of the method followed here is that any material can be used in its pure form, as long as the donor and acceptor materials have a small difference in glass transition temperature (T_g), melting point, or solubility in selective solvents (to avoid erasure of the first imprint during the second imprinting step). F8TBT is an ambipolar polyfluorene polymer, which acts as an electron acceptor in blends with P3HT and as a hole acceptor in blends with PCBM.[19] In both cases external quantum efficiencies (EQE) of over 25% and power conversion efficiencies (PCE) of ~1.2% under simulated sunlight were achieved. Building on our previous work on P3HT:F8TBT devices, we here present devices based on P3HT:PCBM and F8TBT:PCBM.

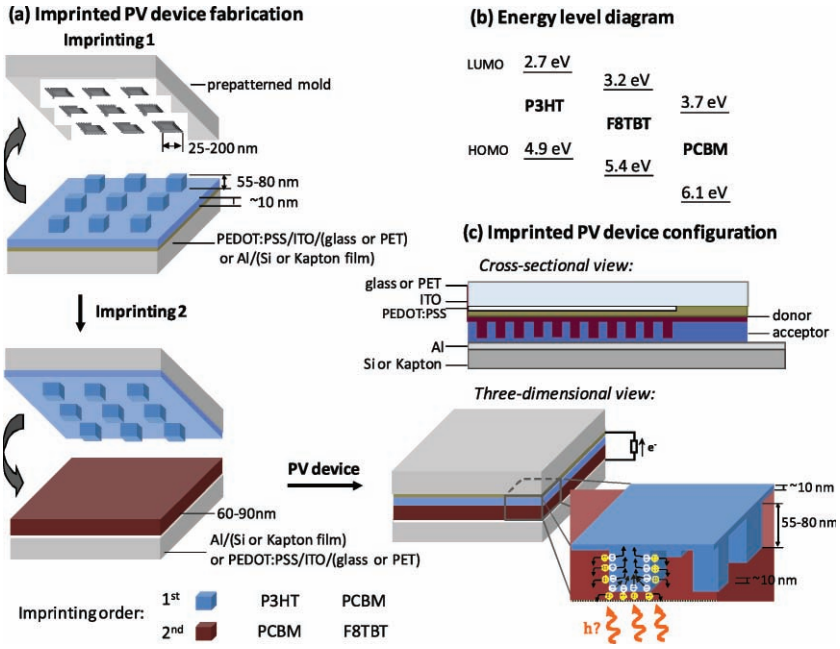

Figure 1. a) Schematic procedure of imprinted PV device fabrication. The imprinting order is illustrated in the figure. Imprinting 1: A Si mold is used to pattern the first film on a suitable substrate, serving as anode or cathode for P3HT:PCBM and F8TBT:PCBM devices, respectively. Imprinting 2: The patterned first film is used as a mold to imprint the second film, resulting in a double-imprinted PV device. The bottom-right drawing shows a 3D close-up cross-sectional view indicating the electron and hole transfer at the interdigitated nanostructured ordered-BHJ. b) Energy level diagram showing the HOMO and LUMO levels of P3HT, F8TBT, and PCBM. c) The cross-sectional view of the double-imprinted PV device containing six 2 mm × 4 mm pixels. The conventional rigid imprinted PV devices are based on glass and Si substrates, while the flexible cells are based on PET and Kapton polyimide films.

1.1. Device Fabrication

The electron donor material (P3HT or F8TBT) was spin-cast on PEDOT:PSS coated ITO/glass or PET substrates, while the electron acceptor material (PCBM) was deposited on a Si substrate or a Kapton film coated with a thermally evaporated Al cathode. Since P3HT is easily oxidized and decomposes at elevated temperatures (usually above 60 C) and PCBM is difficult to imprint by thermal embossing under mild conditions due to its very high melting point, we employed solvent assisted nanoimprint lithography (SANIL)[20], which provides a way to pattern polymer films at room temperature and quite low pressure of only several millibars. The SANIL conditions, especially the solvent vapor saturation and swelling time, were carefully optimized to ensure that residual layers were still present in the patterned films to avoid shorting the devices. In summary, the imprinted P3HT:PCBM devices were fabricated by using SANIL twice, while F8TBT:PCBM devices were imprinted using SANIL and conventional NIL to pattern PCBM and F8TBT, respectively. The order of the two imprinting steps using the same Si molds for P3HT:PCBM and F8TBT:PCBM devices was different (**Figure 1**), because of the varying imprinting requirements of different materials and the volume ratio of pillar and hole arrays. Details of these can be found in the experimental part.

In order to perform a systematic study of the correlation of device performance with feature size and interface area, a series of molds were either fabricated in-house using e-beam lithography or were obtained commercially from NIL Technology ApS. The molds contain 75–80 nm deep 2-D dot patterns with feature sizes of 200, 150, 100, 80, 40, and 25 nm and equivalent spacing (i.e., the pitch is double the feature size) and with patterned area of 4 mm × 2 mm for each pixel. In addition, for some experiments two types of 1-D grating patterns were also used, one with 50 nm wide lines separated by 50 nm gaps, the other with 20 nm wide lines separated by 80 nm gaps. Two types of control cells based on planar bilayers (by non-patterned double imprinting) and standard blend films (by spin-coating from a mixture solution), for both F8TBT:PCBM and P3HT:PCBM systems, were fabricated for comparison. Fabrication procedures are detailed in the Experimental Section.

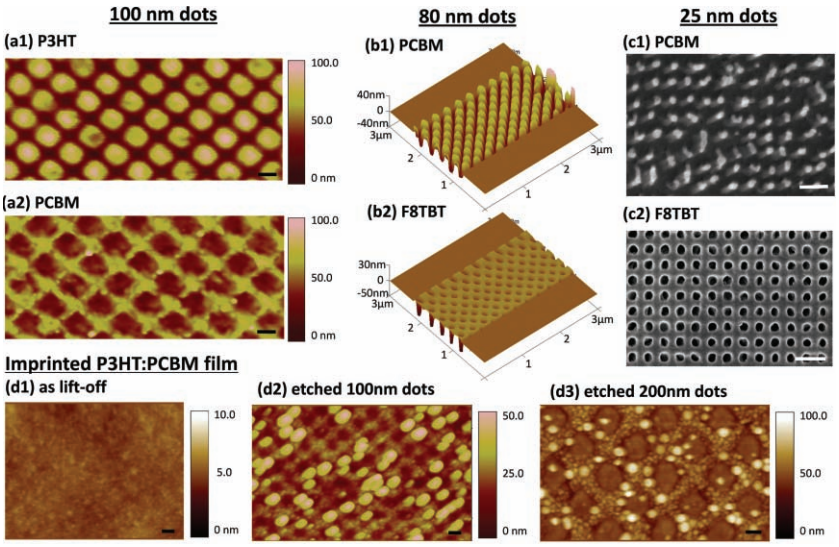

Figure 2. AFM (a1–b2, d1–d3) and SEM (c1, c2) images of double imprinted films. Plan-view AFM images of the (a1) P3HT – (a2) PCBM pair showing an grid of 100 nm wide dots. Similar 3D AFM images of an imprinted grid of 80 nm wide dots; SEM images of the (c1) PCBM–(c2) F8TBT pair showing a square lattice of 25 nm wide dots and holes. (d1)–(d3) Morphologies of double-imprinted bi-layer films of P3HT on top of PCBM after lift-off of the top substrate, before (d1) and after (d2, d3) oxygen plasma etching for 1.2 min (100 W). This removes the top 50 nm of the film, revealing the internal morphology. Feature sizes: 100 nm (d2) and 200 nm (d3) wide dots with 100 nm and 200 nm spacing, respectively. Scan area: 1 m × 3 m. All scale bars: 100 nm.

2. Results and Discussion

2.1. Morphology Studies

Perfect pattern replication was achieved by double imprinting at room temperature **Figure 2** shows the AFM and SEM images of imprinted P3HT, F8TBT, and PCBM films, and the vertical cross-section of an imprinted P3HT/PCBM film. The stamp profile was transferred into the polymer with high fidelity: comparison of the P3HT topography (Figure 2 (a1)) with the imprinted PCBM film (Figure 2 (a2)) shows the clear correspondence of the uniform pillar and hole arrays consisting of 100 nm wide, 80 nm high square dots. The patterned P3HT film after chloroform and dichloromethane vapor annealing and solvent-assisted imprinting the PCBM film was still clear and uniform, indicating that embossing under solvent flow did not deform the nanostructure in the P3HT film, nor did the thermal annealing of the PV cell after imprinting roughen its surface. The features in the P3HT film were fairly well retained even after imprinting the PCBM film and exposure to a selective solvent and ultrasonication to remove the PCBM layer.

To investigate the internal structure of the P3HT/PCBM interface, the top substrate of the sandwich-structured PV cell was lifted off and the top ~60 nm of the double imprinted film was etched off by an oxygen plasma to expose the internal nanostructured P3HT/PCBM layer, where PCBM penetrated into the P3HT grid. The as-exposed film before etching was fairly flat, with a subtle grid pattern, shown in Figure 2 (d1). After plasma etching, the 100 nm and 200 nm grids of P3HT precisely interpenetrating PCBM are clearly revealed in Figure 2 (d2) and (d3), respectively. Also, PCBM clusters or crystallites (elevated dots in Figure 2 (d2) and (d3)) appeared on the surface, because of their low etching rate compared to polymer.[21,22] The clusters also explain why the PCBM film surface in the AFM image (Figure 2 (a2)) was relatively rough.

Figure 2 also shows the 80 nm high 80 nm wide round dots (80 nm spacing) in a PCBM film (b1) that were imprinted into a F8TBT film (b2), and similarly, 80 nm high, 25 nm wide dots (25 nm spacing) in a PCBM film (c1) that were imprinted into F8TBT film (c2). Since the aspect ratio of the 25 nm dots of 1:3.2 was much higher than those of 80 and 100 nm dots (1:1 and 1.25:1), the pillars in the PCBM film were slightly distorted after removing F8TBT by selective solvent and ultrasonication.

2.2. Spectroscopy

During the fabrication of imprinted PV devices, P3HT, F8TBT and PCBM films were patterned by either or both SANIL using chloroform ($CHCl_3$) or dichloromethane (CH_2Cl_2) and/or NIL at an elevated temperature, which involved solvent vapor annealing, thermal annealing, and nano-confinement, followed by thermal annealing of the final integrated internal nanostructured bilayer films. Therefore, it is worthwhile to investigate the effects of solvent/thermal annealing and nanoconfinement on the optical properties of F8TBT and PCBM films and also their influence on PV efficiencies.

2.2.1. UV

Pristine P3HT, F8TBT and PCBM films, and double-imprinted (100 nm dot) and blend P3HT:PCBM and F8TBT:PCBM films were studied by UV–vis spectroscopy, as shown in **Figure 3**.

Consistent with previous reports about annealing and imprinting polymers,[23–25] our previous study[14] has shown that the imprinted P3HT film exposed to solvent vapor has a greater degree of crystallinity than the untreated films. In the UV–vis spectrum of P3HT:PCBM and F8TBT:PCBM films in Figure 3, red-shifts were observed for the imprinted films compared to the blend. Moreover, imprinted P3HT:PCBM films showed a pronounced increase of the shoulder centered at ~610 nm, the intensity of which is correlated with the degree of P3HT crystallinity. These are attributed to an enhanced conjugation length and more ordered structure of P3HT, which were induced by self-organisation of the mobile chains during solvent swelling or under heating.[26] Compared to P3HT, F8TBT is less crystalline. The thermal annealing during and after imprinting mainly helped to remove residual solvent and reduce the free volume, which could lead to closer packing of the polymer chains[27] and has been shown to lead to an improvement in hole mobility.[28] The stronger absorption at 530 nm in the imprinted

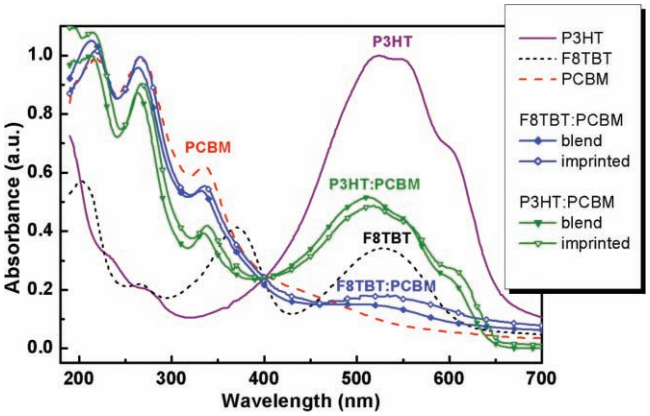

Figure 3. Absorption spectra of imprinted P3HT, F8TBT and PCBM films, double-imprinted films and blend films made from solution mixtures of P3HT:PCBM and F8TBT:PCBM.

F8TBT:PCBM film as shown in Figure 3 provides some indication of improved packing of the F8TBT.

2.2.2. PL

PL measurements (**Figure 4**) showed strong quenching in both imprinted F8TBT:PCBM and P3HT:PCBM films, and a decrease of PL intensity as pattern feature size decreased from 80 nm to 25 nm. Very strong PL quenching (by 86% in comparison to pure P3HT at 713 nm) was observed in the double imprinted films with 25 nm features (i.e. max. distance to D/A interface: 12.5 nm), strongly indicating that these dimensions are comparable to the exciton diffusion length of ~10 nm in P3HT.[29,30] Even stronger PL quenching (in comparison to pure F8TBT at 653 nm) was measured in the imprinted F8TBT:PCBM film with the same feature size as in the imprinted P3HT:PCBM film. The PL quenching in the imprinted (25 nm) F8TBT:PCBM film (by 92% in comparison to pure F8TBT at 653 nm) was found to be even higher than in a spin-coated blend control film (by 90%). This improved quenching might indicate a larger exciton diffusion length in F8TBT than in P3HT. However, both F8TBT and P3HT might remain slightly mixed with PCBM after phase separation and PCBM might also diffuse into the polymer layers. Any phase impurity would contribute to the PL quenching of the polymer even at feature sizes significantly larger than the exciton diffusion lengths.

Overall, the spectroscopy data indicate that the patterning procedure resulted in favorable nanoscale morphologies of the photoactive layers for the dissociation of excitons and the transport of charge carriers, which are prerequisites for the improvement of PV efficiencies.[31]

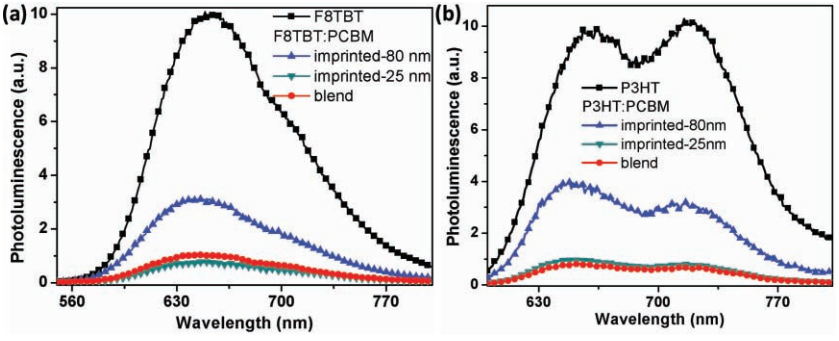

Figure 4. Photoluminescence (PL) spectra of pristine F8TBT and P3HT films, blend films, and imprinted F8TBT:PCBM and P3HT:PCBM films with feature sizes of 80 and 25 nm. Excitation wavelengths for PL measurements are 550 nm for F8TBT and F8TBT:PCBM films and 520 nm for P3HT and P3HT:PCBM blend films.

2.3. Device Performance

2.3.1. F8TBT-PCBM

Figure 5 shows the EQE and current–voltage (J–V) characteristics of the double-imprinted PV cells for a series of feature sizes in comparison to planar and blend controls under solar illumination conditions. There is an obvious correlation of pattern feature sizes (or D/A interface areas) with EQE and PCE, short circuit current density (J_{SC}) and fill factor (FF). Device performance parameters are also summarized in **Table 1**.

As recorded in **Table 2**, the open circuit voltage (V_{OC}) of nanostructured PV cells is in the range of 1.04–1.17 V, while that of blend control device is only 1.01 V which might be attributed to the reduced F8TBT:PCBM ratio (1:5 by weight) compared to the ratio used in previously reported blend cells (1:3 by weight, V_{OC} = 1.1 V)[19] and the absence of thermal annealing.

The comparison showed that both 1D and 2D patterns of well-ordered densely packed gratings and dots in imprinted PV cells, with increased D/A interface areas compared to that of bilayer cells, significantly enhanced the device performance. The influence of pattern feature size and D/A interface area on the key PV parameters including EQE, PCE, J_{SC}, and FF are plotted in Figure 5c and d. As shown in Figure 5c, EQE and PCE increased steadily as the feature size decreased, consistent with improved exciton dissociation. As shown in Figure 5d, J_{SC} increased over 3-fold when the interface area increased 4-fold from planar to 25 nm-dot patterned interface. In a simple model where the short-circuit current is limited by exciton dissociation, J_{SC} would be expected to scale approximately linearly with interfacial area. Detailed comparison (Figure 5d) shows a more complex behavior, with little additional short-circuit current to be gained below a feature size of 80 nm, despite the fact that the PL is not completely quenched in imprinted structures with an 80 nm feature size. Factors other than exciton dissociation based on interfacial area must therefore play a role in determining the yield of collected carriers. This is also evidenced by the comparison between 1D and 2D patterned PVs. As illustrated in Table 2, the devices with 50 nm and 20 nm wide (100 nm pitch) 1D line arrays have 2.6 times higher D/A interface area than the planar bilayer control device, however their performance is considerably lower than that of the 2D patterned devices with equivalent interface area.

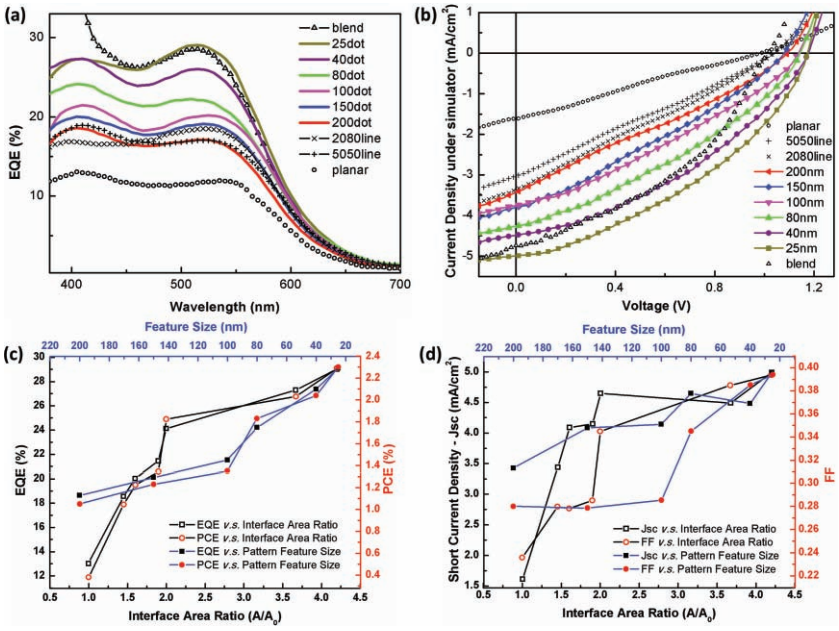

Figure 5. a) EQE and b) *J–V* characteristics of the double-imprinted F8TBT-PCBM PV cells for a series of feature sizes in comparison to planar and blend controls under solar illumination conditions. Correlation of pattern feature sizes or D/A interface areas with (c) EQE (low intensity) and PCE, and (d) J_{SC} and FF.

An important feature of the 2D nanoimprinted devices is their improved V_{OC} with respect to the blend devices. This might be attributed to a reduction in shunt losses, due to the presence of correctly arranged wetting layers in the imprinted devices. However this mechanism does not explain the low V_{OC} seen in the bilayer device, which should also prevent carriers from escaping at the wrong electrode. The fill-factor increases as the feature size decreases, reaching a value of 0.39 for 25 nm features, identical to that achieved in the blends. The fill factor is often determined by the field required to separate bound geminate charge pairs formed at the heterojunction into free carriers, although it can be influenced by bimolecular recombination or space-charge effects at high intensities or where geminate pair separation is particularly facile. Modeling predicts that geminate separation should be suppressed in fine blends where carriers are confined by the blend structure, whereas both bilayers and interdigitated structures should give similarly good geminate separation, in contradiction to the results presented here. This suggests that more subtle effects such as modifications of interfacial recombination rates or local mobilities are playing an important role in the imprinted structures.

Compared to blend control device, the PV devices with 40 and 25 nm wide dot features both have higher PCEs, as a consequence of good charge collection combined with improved open-circuit voltage. For an exciton diffusion length of around 10 nm in F8TBT,[32] it is unlikely that the exciton quenching is complete in the 40 nm structure. The fact that this structure nevertheless gives good efficiencies indicates that nanoimprinted structures can give particularly favorable conditions for charge separation and charge collection.

2.3.2. P3HT-PCBM

The same series of 2D patterned molds were also used to fabricate PV devices based on P3HT and PCBM (**Figure 6**). As shown in Figure 6b, the imprinted P3HT:PCBM cells did not present significant enhancement of V_{OC}, as observed in F8TBT:PCBM cells, compared to their blend control devices. The V_{OC} of imprinted and control P3HT:PCBM cells were all around 0.6 V, which are comparable to reported values.[33–36] The similarity in V_{OC} of the imprinted and standard blend P3HT:PCBM devices could be explained by the well evolved morphology in blend devices upon annealing, resembling the idealized PV structure, through favorable vertical diffusion of P3HT and PCBM to their corresponding electrodes.[9] In contrast, this favorable structure has not been reported in the F8TBT:PCBM system described above, which might be due to the relatively poor crystallinity of the amorphous polymer F8TBT compared to P3HT. The double imprinting approach would hence be most beneficial for less ordered, less crystalline materials.

Figure 6c shows that EQE increases steadily as the feature size is decreased. Just as in the F8TBT:PCBM devices, the EQE does not scale linearly with D/A interface area, becoming less sensitive to interface area below a feature size of 80 nm. The PCE increases with reducing feature size, reaching a value of 3.25% for 25 nm features, despite a slight drop in fill factor at this size that might be attributed to difficulties in charge separation due to slight distortion and non-uniformity of nanostructures with very high aspect ratios. The 1D imprinted structures again perform less well than would be predicted based on their interfacial area. We note that a recent study on the crystallinity

Table 1. Photoluminescence intensities of pristine F8TBT and P3HT films, blend films, and imprinted F8TBT:PCBM and P3HT:PCBM films with feature sizes of 80 and 25 nm.

	PL intensity (a.u.) at 653 nm quenching				PL intensity (a.u.) at 716 nm quenching			
	F8TBT	10	–		P3HT	10	–	
F8TBT:PCBM	imprinted 80 nm	3.1	69%	P3HT:PCBM	imprinted 80 nm	3.5	65%	
F8TBT:PCBM	imprinted 25 nm	0.8	92%	P3HT:PCBM	imprinted 25 nm	1.4	86%	
F8TBT:PCBM	blend	1.0	90%	P3HT:PCBM	blend	1.2	88%	

Table 2. Summary of device performance of F8TBT:PCBM photovoltaic devices.

	Feature Size–width [nm]	A/A_0 [mm^2][a)]	Max. EQE [%]	V_{OC} [V]	J_{SC} [mA cm^{-2}]	FF	PCE [%][b)]
Planar	–	1	13.0	1.00	1.61	0.24	0.38
Imprinted line (width–space)	50–50	2.60	18.5	1.04	2.83	0.28	0.82
	20–80	2.60	18.9	1.04	3.13	0.28	0.92
Imprinted dot (width=space)	200	1.45	18.6	1.09	3.44	0.28	1.05
	150	1.60	20.0	1.08	4.09	0.28	1.23
	100	1.90	21.5	1.14	4.15	0.29	1.35
	80	2.00	24.1	1.14	4.26	0.35	1.69
	40	3.67	27.3	1.18	4.49	0.39	2.04
	25	4.20	29.0	1.17	4.99	0.39	2.30
Blend	–	–	28.5	1.01	4.78	0.39	1.90

[a)] A/A_0 is the ratio of D/A interface areas of the patterned to the planar-interface PV devices. [b)] Illumination intensity equivalent to 100 mW cm^{-2} after spectral mismatch correction using AM 1.5G solar simulator.

of P3HT in nanoconfinement induced by nanoimprinting proposed that 1D grating and 2D pillars had different polymer chain alignment forms, respectively leading to a laterally lamellar form (backbone parallel and side-chains perpendicular to the substrate) and an axis orientation form (orientation axially aligned with the pillar center).[25] This potential difference in the alignment of P3HT might be responsible for the differences in device performance between the 1D and 2D imprinted layers seen here.

Unlike F8TBT, P3HT is rather sensitive to oxygen and humidity. Currently, our double imprinting fabrication cannot be conducted entirely in a glove box as the solvent-assisted nanoimprinter is placed in the open. Although a stream of nitrogen flows through the sample holder, the exposure to air during sample transfer to the glove box before device encapsulation has effects on the aluminum electrode and P3HT. Oxidation could well reduce the performance of the imprinted cells, as suggested by the reduction in PCE of a blend control cell that had been exposed to air for 20 min after spin-coating before electrode deposition (**Table 3**). The performance of the 25 nm 2D imprinted device does not quite match that of the pristine blend control device, but is better than that of the blend device exposed to air, again indicating that nanoimprinting leads to a highly favorable structure for exciton dissociation and charge collection. We believe that further improvements in efficiency could be achieved if the thickness of the nanostructured layer could be increased so as to absorb more light. This is particularly relevant in P3HT:PCBM devices where only the columns in the imprinted region are absorbing. It is, however, challenging to achieve aspect ratios higher than the values reported here.

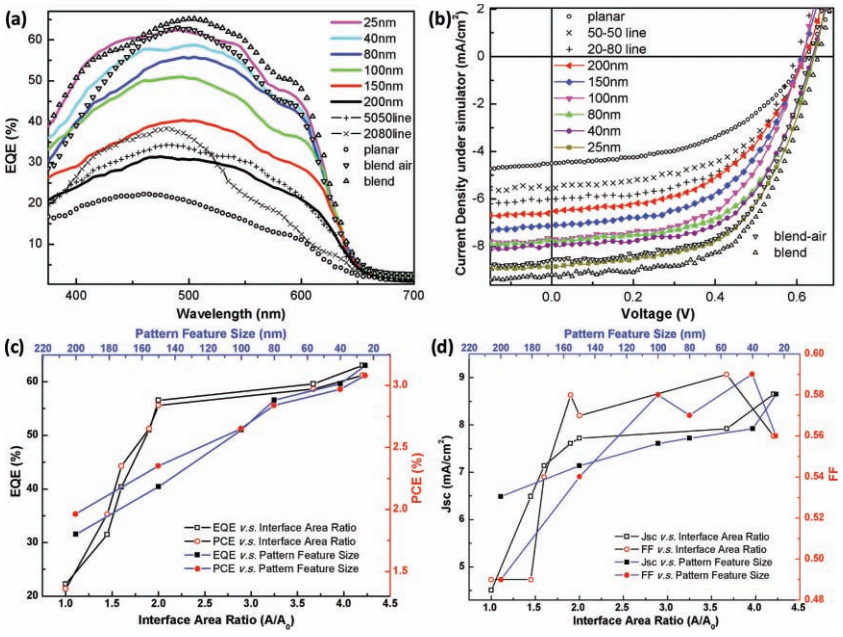

Figure 6. a) EQE and b) *J–V* characteristics of the double-imprinted P3HT-PCBM PV cells for a series of feature sizes in comparison to planar and blend control cells under solar illumination conditions. The correlation of pattern feature sizes or D/A interface areas with (c) EQE (low intensity) (-○-), PCE (-■-), (d) J_{sc} (-○-) and FF (-■-).

3. Conclusion

We have shown how double imprinting using a nanoimprinted polymer film to imprint another organic layer by NIL generated interdigitated D/A films with feature sizes down to 25 nm. AFM and SEM provide clear evidence that the features in the polymer mold used in the second imprinting step are not, or only minimally distorted during imprinting. We studied the photovoltaic device performance of nanostructured films based on P3HT or F8TBT as donor polymers and PCBM as acceptor material and studied in both cases the influence of feature size and interfacial area on device performance. The results provide

Table 3. Summary of device performance of P3HT:PCBM photovoltaic devices.

	Feature Size –width [nm]	A/A_0 [mm^2][a)]	Max. EQE [%]	V_{OC} [V]	J_{SC} [mA cm^{-2}]	FF	PCE [%][b)]
Planar	–	1.00	22.3	0.62	4.51	0.49	1.36
Imprinted line (width–space)	50–50	2.60	34.3	0.62	5.52	0.53	1.82
	20–80	2.60	38.3	0.61	5.97	0.55	2.01
Imprinted dot (width=space)	200	1.45	31.5	0.62	6.49	0.49	1.96
	150	1.60	40.4	0.61	7.14	0.54	2.35
	100	1.90	51.0	0.61	7.61	0.58	2.65
	80	2.00	56.5	0.64	7.72	0.57	2.84
	40	3.67	59.6	0.64	7.92	0.59	2.97
	25	4.20	63.0	0.64	8.65	0.56	3.25
Blend	–	–	65.1	0.65	9.18	0.59	3.50
Blend in Air	–	–	63.0	0.63	8.57	0.59	3.20

[a)] A/A_0 is the ratio D/A of interface areas of the patterned to the planar-interface PV devices. [b)] Illumination intensity equivalent to 100 mW cm^{-2} after spectral mismatch correction using AM 1.5G solar simulator.

direct evidence that the exciton diffusion range in these systems is comparable to the smallest spacings (around 25 nm) we have studied here. The double-imprinted films facilitate charge transport as well as charge separation, and led to additional ordering of the conjugated polymer. An additional benefit of this method is that both donor and acceptor layers completely cover the correct electrode. By changing the imprint pattern, double imprinting has the potential to independently tailor the dimensions of *both* phases to match the exciton diffusion lengths in both phases. As the double imprinting process is suitable for a very wide range of materials, it should be possible to investigate many more combinations of donor and acceptor materials. The advantage of such an approach is the study of the electronic properties of different materials combinations using identical device morphologies, which is impossible for spin-cast blends. Any change in device performance can then be systematically compared and correlated to the molecular structure of the active materials.

4. Experimental Section

Materials: Regioregular P3HT ($M_w = 8.7 \times 10^4$ g mol^{-1}) was purchased from Merck Chemicals and used after purification by Soxhlet extraction. F8TBT ($M_w = 5.3 \times 10^4$ g mol^{-1}) was synthesized at the Melville Laboratory, University of Cambridge. PCBM was purchased from from Nano-C and used as obtained.

Device Fabrication: 65–85 nm thick P3HT and F8TBT films were spin-cast from $CHCl_3$ solution (both 10 mg mL^{-1}) onto PEDOT:PSS coated ITO/glass substrates, while 80 nm PCBM films were deposited onto Si or Kapton polyimide film substrates coated with thermally evaporated Al cathodes (80 nm thick). *For P3HT:PCBM PV devices*: P3HT films were imprinted by SANIL using a sequence of swelling the sample in a saturated $CHCl_3$ vapor:nitrogen (9:1) flow (50 sccm) for 30–50 min, imprinting at room temperature by a Si mold for 20 min, and then quenching by N_2 flow (20 sccm) for 60 min, followed by annealing at 120 C for 5 min in a glove box to remove residual solvent. Subsequently, PCBM films were imprinted by previously patterned P3HT films using SANIL following the same procedure with a saturated CH_2Cl_2 vapor:N_2 (9:1) flow (50 sccm). Imprinted PV cells were annealed at 120 C for 10 min after the second printing. For control devices, P3HT:PCBM planar bilayer control devices were fabricated by similar procedure, using the solvent assistant imprinter with unpatterned P3HT films pressed onto PCBM films under the exactly same conditions described above. P3HT:PCBM blend control devices were fabricated by spin-coating 70 nm thick P3HT:PCBM blend (1:0.8 by weight) films from dichlorobenzene solution, followed by annealing at 120 C for 5 min and subsequent thermal evaporation of 100 nm Al electrodes. *For F8TBT:PCBM PV Devices:* PCBM films were imprinted by SANIL under same conditions as imprinting P3HT films described above. Subsequently, the patterned PCBM films were used as molds to imprint into F8TBT films using conventional NIL, i.e., thermal embossing at 115 C under 30 bar for 10 min. The imprinted assembly was then annealed at 120 C for 15 min. F8TBT:PCBM planar bilayer control devices were fabricated using a similar procedure, where unpatterned PCBM films were pressed onto F8TBT films via thermal embossing under the same conditions as described above. F8TBT:PCBM blend control devices were fabricated by spin-coating 70 nm thick F8TBT:PCBM blend (1:5 by weight, mixed from F8TBT in tetrachlorobenzene and PCBM in chloroform) films, followed by annealing at 120 C for 5 min and subsequent thermal evaporation of 100 nm Al electrodes. In order to examine the effect of air on PV performance, some blend control cells were exposed to air for 20 min after spin-coating and Al electrode deposition. All devices were encapsulated in epoxy resin in the glove box for device testing.

Device Testing: Current-voltage (*J*–*V*) characteristics were measured in air at room temperature using a Keithley 237 source-measure unit. The photocurrent spectra were recorded by illumination from a Xenon lamp dispersed through a single-grating monochromator. The current-voltage characteristics under AM1.5G illumination were measured using a solar simulator (Oriel Instruments 81160) at an intensity equivalent to 100 mW cm^{-2} after correction for spectral mismatch.

Acknowledgements

This work was supported by the Engineering and Physical Science Research Council. X.H. was supported by the Gates Cambridge Trust.

Received: March 25, 2010
Published online: November 9, 2010

[1] J. Peet, A. J. Heeger, G. C. Bazan, *Acc. Chem. Res.* **2009**, *42*, 1700.
[2] S. H. Park, A. Roy, S. Beaupre, S. Cho, N. Coates, J. S. Moon, D. Moses, M. Leclerc, K. Lee, A. J. Heeger, *Nature Photon.* **2009**, *3*, 297.
[3] H. Y. Chen, J. Hou, S. Zhang, Y. Liang, G. Yang, Y. Yang, L. Yu, Y. Wu, G. Li, *Nature Photon.* **2009**, *3*, 649.
[4] D. Vacar, E. S. Maniloff, D. W. McBranch, A. J. Heeger, *Phys. Rev. B* **1997**, *56*, 4573.
[5] K. Brunner, A. Tortschanoff, Ch. Warmuth, H. Bässler, H. F. Kauffmann, *J. Phys. Chem. B* **2000**, *104*, 3781.
[6] J. J. M. Halls, K. Pichler, R. H. Friend, S. C. Moratti, A. B. Holmes, *Appl. Phys. Lett.* **1996**, *68*, 3120.
[7] X. Yang, J. Loos, Macromolecules, **2007**, *40*, 1353.
[8] G. Li, V. Shrotriya, J. Huang, Y. Yao, T. Moriarty, K. Emery, Y. Yang, *Nat. Mater.* **2005**, *4*, 864.
[9] M. Compoy-Quiles, T. Ferenczi, T. Agostinelli, P. G. Etchegoin, Y. Kim, T. D. Anthopoulos, P. N. Stavrinou, D. C. Bradley, J. Nelson, *Nat. Mater.* **2008**, *7*, 158.
[10] Y. Zhao, Z. Xie, Y. Qu, Y. Geng, L. Wang, *Appl. Phys. Lett.* **2007**, *90*, 043504.
[11] J. Peet, J. Y. Kim, N. E. Coates, W. L. Ma, D. Moses, A. J. Heeger, G. C. Bazan, *Nat. Mater.* **2007**, *6*, 497.
[12] R. G. Alargova, S. Deguchi, K. Tsujii, *J. Am. Chem. Soc.* **2001**, *123*, 10460.
[13] K. M. Coakley and M. D. McGehee, *Chem. Mater.* **2004**, *16*, 4533.
[14] X. He, F. Gao, G. Tu, D. Hasko, S. Huttner, U. Steiner, N. C. Greenham, R. Friend, W. T. S. Huck, *Nano Lett.* **2010**, *10*, 1302.
[15] M. Kim, J. Kim, J. C. Cho, M. Shtein, L. J. Guo, J. Kim, *App. Phys. Lett.* **2007**, *90*, 123113.
[16] M. Aryal, F. Buyukserin, K. Mielczarek, X. Zhao, J. Gao, A. Zakhidov, W. Hu, *J. Vac. Sci. Technol. B* , **2008**, *26*, 2562.
[17] C. Goh, K. M. Coakley, M. D. McGehee, *Nano Letters* **2005**, *5*, 1545.
[18] K. M. Coakley, Y. X Liu, M. D. McGehee, *Adv. Funct. Mater.* **2003**, *13*, 301.
[19] C. R. McNeill, A. Abrusci, J. Zaumseil, R. Wilson, M. J. McKiernan, J. H. Burroughes, J. J. M. Halls, N. C. Greenham, R. H. Friend, *App. Phys. Lett.* **2007**, *90*, 193506.
[20] N. E. Voicu, S. Ludwigs, E. J. W. Crossland, P. Andrew, U. Steiner, *Adv. Mater.* **2007**, *19*, 757.
[21] Y. G. Kim, B. C. Thompson, N. Ananthakrishnan, G. Padmanaban, *J. Mater. Res.* **2005**, *20*, 3188.
[22] H. Hoppe, M. Niggemann, C. Winder, J. Kraut, R. Hiesgen, A. Hinsch, D. Meissner, N. S. Saricifci, *Adv. Funct. Mater.* **2004**, *14*, 1005.
[23] T. Guo, T. Wen, G. L. Pakhomov, X. Chin, S. Liou, P. Yeh, C. Yang, *Thin Solid Films* **2008**, *516*, 3138.
[24] R. Österbacka, C. P. An, X. M. Jiang, Z. V. Vardeny, *Science* **2000**, *287*, 839.
[25] M. Aryal, K. Trivedi, W. Hu, *ACS Nano* **2009**, *3*, 3085.
[26] Y. Zhao, Z. Xie, Y. Qu, Y. Geng, L. Wang, *App. Phy. Lett.* **2007**, *90*, 043504.
[27] T. W. Holcombe, C. H. Woo, D. F. Kavulak, B. C. Thompson, J. M. J. Fréchet, *J. Am. Chem. Soc.* **2009**, *131*, 14160.
[28] F. Padinger, R. S. Rittberger, N. S. Sariciftci, *Adv. Funct. Mater.* **2003**, *13*, 85.
[29] L. Lüer, H. J. Egelhaaf, D. Oelkrug, G. Cerullo, G. Lanzani, B. H. Huisman, D. de Leeuw, *Org. Electron.* **2004**, *5*, 83.
[30] P. E. Shaw, A. Ruseckas, I. D. W. Samuel, *Adv. Mater.* **2008**, *20*, 3516.
[31] E. Klimov, W. Li, X. Yang, G. G. Hoffmann, J. Loos, *Macromolecules* **2006**, *39*, 4493.
[32] C. R. McNeill, J. J. M. Halls, R. Wilson, G. L. Whiting, S. Berkebile, M. G. Ramsey, R. H. Friend, N. C. Greenham, *Adv. Funct. Mater.* **2008**, *18*, 2309.
[33] S. Miller, G. Fanchini, Y. Lin, C. Li, C. Chen, W. Su, M. Chhowalla, *J. Mater. Chem.* **2008**, *18*, 306.
[34] Y. Zhao, Z. Xie, Y. Qu, Y. Geng, L. Wang, *App. Phys. Lett.* **2007**, *90*, 043504.
[35] W. Ma, C. Yang, X. Gong, K. Lee, A. J. Heeger, *Adv. Funct. Mater.* **2005**, *15*, 1617.
[36] J. Kim, S. Kim, H. Lee, K. Lee, W. Ma, X. Huong, A. J. Heeger, *Adv. Mater.* **2006**, *18*, 572.